Received: 1 July 2022 | Revised: 16 July 2022 | Accepted: 22 July 2022

DOI: 10.1111/ijac.14185

International Journal of Applied Ceramic TECHNOLOGY
Ceramic Product Development and Commercialization

SPECIAL ISSUE ARTICLE

Hierarchical microstructure growth in a precursor-derived SiOC thin film prepared on silicon substrate

Emmanuel III Ricohermoso[1] | **Eva Heripre**[2] | **Susana Solano-Arana**[3] | **Ralf Riedel**[1] | **Emanuel Ionescu**[1,4]

[1]Fachbereich Material–und Geowissenschaften, Technische Universität Darmstadt, Darmstadt, Germany

[2]LMPS–Laboratoire de Mécanique Paris-Saclay, Université Paris-Saclay, ENS Paris-Saclay, Gif-sur-Yvette, France

[3]Fachbereich Elektrotechnik und Informationstechnik, Technische Universität Darmstadt, Darmstadt, Germany

[4]Fraunhofer IWKS, Digitalization of Resources Department, Alzenau, Germany

Correspondence
Emmanuel III Ricohermoso and Emanuel Ionescu, Fachbereich Material- und Geowissenschaften, Technische Universität Darmstadt, Otto-Berndt-Str. 3, D-64287 Darmstadt, Germany.
Email: emmanuel_iii.ricohermoso@tu-darmstadt.de; emanuel.ionescu@iwks.fraunhofer.de

Funding information
German Science Foundation (DFG Germany), Grant/Award Number: 411658150; German Science Foundation (DFG Germany),, Grant/Award Number: 411658150

Abstract

Silicon oxycarbide film deposited on a silicon substrate has shown superior electrical conductivity relative to its monolithic counterpart. In this work, the evolution of different microstructures detected on the SiOC film reveals its hierarchical microstructure. The existence of sp^2-hybridized carbon domains has been unambiguously confirmed by means of Raman spectroscopy and transmission electron microscopy corroborated with electron energy loss spectroscopy. The diffusion coefficient of carbon in silica and its dependence on temperature were studied by assessing energy-dispersive X-ray spectroscopy profiles taken from the cross-sections of samples annealed at temperatures in the range from 1100°C to 1400°C. The activation energy for diffusion of carbon in silica was determined to be approximately 3.05 eV, which is significantly lower than the values related to the self-diffusion of silicon and oxygen. The microstructural evolution of precursor to SiC_nO_{4-n} and SiC serves as migration path of sp^2-hybridized carbon to the SiO_x layer. With increasing temperature, the formation of microscale carbon-rich segregation is promoted while the SiOC film becomes thinner.

KEYWORDS
carbon segregation, growth kinetics, polymer-derived ceramics, thin films

1 | INTRODUCTION

Silicon oxycarbide (SiOC) is a type of amorphous ceramics that is preparatively accessible from polysiloxane precursors and can be described as a glassy network consisting of the corner-sharing tetrahedra of $SiO_{4-x}C_x$ (x = 0–4)[1]; consequently, silicon oxycarbide may be considered as silicate-based glasses in which oxygen has been partly replaced by carbon. Multiple studies using different characterization methods, including IR spectroscopy, Raman spectroscopy, XRD, NMR spectroscopy, TGA/MS, and TEM, have been conducted to understand the (thermal) polysiloxane-to-SiOC transformation and to elucidate the structure of SiOC as well as its evolution at different thermal treatment stages.[1–15] Initially, the polysiloxane can be cross-linked via hydrosilylation, free-radical initiation, or condensation, which can be assisted with catalysts such as peroxides and metal acetylacetonates. Polymer-to-ceramic conversion of the cross-linked polysiloxane initiates at 400–600°C upon the evolution of hydrogen and hydrocarbons, mainly CH_4.[5,16–18] Pyrolysis at 600–1100°C results in continuous cleavage of the Si-O, Si-C, and C-H bonds producing free carbons with an onset at 800°C in an amorphous silicon oxycarbide ceramic phase.[19,20] Bois et al. explained with the use of solid-state[29] Si MAS NMR that the glassy network of the SiOC continuously evolves in the temperature range of 1200–1600°C.[21] At 1500°C, the evolution of β-SiC and an sp2 -hybridized segregated carbon phase has been confirmed by XRD analysis.[22,23]

A significant amount of literature is available on the synthesis approach and characterization of SiOC, although the majority is dedicated to powder and monolithic samples. In our latest work on SiOC thin film deposited on a silicon substrate, the evolution of the SiC and free carbon phases were documented at a temperature of 1400°C.[24,25] A micro-scale segregation of phases was observed on the surface of the film; the segregations were found to consist of sp[2-h]ybridized carbon and nanocrystalline β-SiC dispersed within an amorphous silicon oxycarbide matrix. The Si-O-C system is known to follow two processes when exposed to temperatures well beyond 1000°C: The first process involves the partitioning of the glassy $SiO_{4-x}C_x$ network and the formation of amorphous silica and SiC nanodomains, latter may crystallize; the second process represents the carbothermal reaction between the phase-separated silica and the excess carbon, complemented by the growth of crystalline SiC and release of gaseous CO.[9] These processes were extensively studied and are relatively well understood for monolithic SiOC. While they are still scarcely understood for polymer-derived SiOC thin films, as in this case, the substrate may have a significant impact on the phase separation and carbothermal decomposition of SiOC.

The specifics of the present work comprise a thorough investigation of the phases present on the SiOC thin film and first insights related to their segregation and growth. Multiple techniques, including Raman spectroscopy, TEM coupled with EDS, and EELS, were used to further understand the growth kinetics of the C-rich phase segregation in the SiOC-based film. The diffusivity of carbon to the SiO_x layer was carefully assessed and correlated to the formation and the growth of the C-rich segregation within the film.

2 | MATERIALS AND METHOD

2.1 | Materials

Polyramic® SPR 212, a commercially available polysiloxane (Starfire Systems Ltd., Glenville, NY, USA), was used as a polymer precursor for the synthesis of the SiOC thin films. In order to provide an effective crosslinking process of the polymeric films, free radical initiation was catalyzed with 1 wt% of dicumyl peroxide (added as a 50 wt% solution in toluene). A supplementary amount of toluene was added to achieve a 40% dilution of the polymers before the spin-coating deposition.

A 100-mm diameter boron-doped p-type Si (100) wafer with 525 μm thickness (Prime Si + SiO_2, MicroChemicals GmbH, Ulm, Germany) was chosen as the substrate. The Si substrates have a SiO_2 passivation layer with a thickness of ≈500 nm grown in successive dry-wet-dry oxidation processes.

2.2 | Thin film preparation

In a cleanroom, spin coating was performed using LabSpin 8 (Süss MicroTec SE, Garching, Germany) with a static dispense technique. A cascading technique of sequential acetone and isopropanol was used to clean the surface of the Si substrate prior to precursor deposition. The spin coating process was optimized concerning three main parameters: (1) initial spin speed, (2) acceleration profile, and (3) final spin speed. Using the Taguchi method, the design of experiment was carried out with the film thickness as the response factor. The film thickness was determined using a profilometer (Dektak XT Advanced System, Brucker, Karlsruhe, Germany) and measured in three different positions for each sample. The full details of the optimization process including the statistical approach are reported in detail in Reference 24. A favorable response was obtained using the setting of an initial spin speed of 4000 rpm for 30 s, then accelerated to a second spin speed of 8000 rpm for 30 s with an acceleration of 500 rpm/s.

The samples were thermally cross-linked at 250°C in air on a direct-contact hot plate. Subsequently, the samples were pyrolyzed in a graphite crucible placed in a high-temperature furnace (FCT-Uniaxial hot-press, FCT Systeme GmbH, Frankenblick, Germany) under a high purity nitrogen atmosphere. The thermal profile involved heating to 1100°C with a rate of 100 K min^{-1} followed by a dwell time of 2 h. Finally, the samples were annealed at different temperatures, 1200°C, 1300°C, or 1400°C with dwell times of 1, 2, or 3 h before cooling down to room temperature.

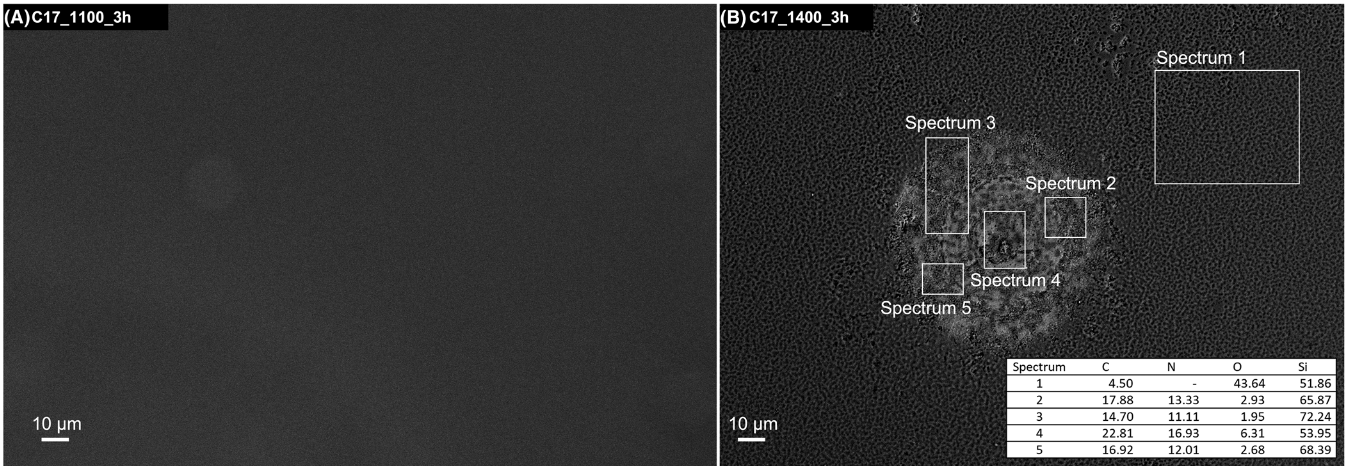

FIGURE 1 Backscattered SEM micrograph of C17_1400_3h sample with five EDS spectra. Spectrum 1 is taken on the matrix of the film while Spectra 2–5 were taken on the particle.

For nomenclature, the prepared samples are labeled following the format of *C17_Annealing temperature_Dwell time*. In this case, C17 stands for the 17 wt% free carbon content of the sample.

2.3 | Characterization

The SiOC thin film deposited on a silicon substrate was cut into 1×1 cm^2 coupons for characterization purposes. The samples were primarily characterized by Raman Spectroscopy (LabRAM Horiba HR Raman Spectroscope HR800, Horiba Jobin Yvon GmbH, Bensheim, Germany), scanning electron microscopy [SEM] coupled with energy dispersive spectroscopy [EDS] (JEOL JSM 7600F, JEOL Ltd., Chiyoda, Tokyo, Japan).

For the cross-section preparation of the thin-film specimens, a Helios Nanolab 660 scanning electron microscope (FEI Thermofischer) was used in combination with a high-precision ion milling using FIB. A Titan3 G2 80–300 microscope (FEI Thermofisher) with probe (STEM) and conventional TEM modes was used to analyze the prepared sample. The device was coupled with EDS analysis and an Enfinium EELS detector (Gatan) with a resolution of 0.8 eV.

3 | RESULTS AND DISCUSSION

The morphology of the prepared SiOC-based thin films was studied by means of SEM as shown in Figure 1. A homogeneous SiOC film is clearly seen in Figure 1A with no manifestation of carbon segregation. Based on the backscattered SEM micrograph shown in Figure 1B, a clear indication of compositional differences was seen on the surface of the C17_1400_3h sample. Through EDS analysis, five areas were selected and the composition of each spectrum (element fraction given in wt%), was recorded and is shown as an inset in Figure 1. Spectrum 1 revealed that a high concentration of oxygen is present in the matrix of the film, while Spectra 2–5 are carbon-rich and oxygen-deficient. Nitrogen is also present within the formed segregation which can originate from the annealing atmosphere.

The sp[2-h]ybridized carbon was shown to be present in both the SiOC matrix as well as in the oxygen-depleted segregations and was extensively studied by means of Raman spectroscopy. Raman analysis has been identified as a suitable non-destructive characterization technique for carbon and carbon-based materials where every band of the spectrum corresponds to a specific vibrational frequency of a molecular bond. In particular, carbon materials are typically characterized by three major bands in the Raman spectrum, namely the G-band, the D-band, and the 2D-band. The G-band is denoted as the characteristic band of graphene at 1582 cm^{-1}, which is a result of the only Raman active E_{2g} mode at the Γ point. The E_{2g} mode is doubly degenerate optical vibration where carbon atoms move in graphene planes.[26–28] In a graphitic material, the three-dimensional lattice built from layers of graphene, the zone centers are given by $\Gamma^{graphite} = 2A_{2u} + 2B_{2g} + 2E_{1u} + 2E_{2g}$. This results in two Raman-active modes at the Γ point at 1582 cm^{-1} and at 44 cm^{-1}. The other prominent peaks on the Raman spectrum belong to the disorder-induced bands within the material. D-band on the other hand is the double-resonant Raman process caused by hybridized vibrational mode at the edges of graphene.[29] The second-order peak, the 2D-band (also called D* or G′), is a result of the longitudinal optical branches of graphite in an over bent state. Detailed work on the assignment of

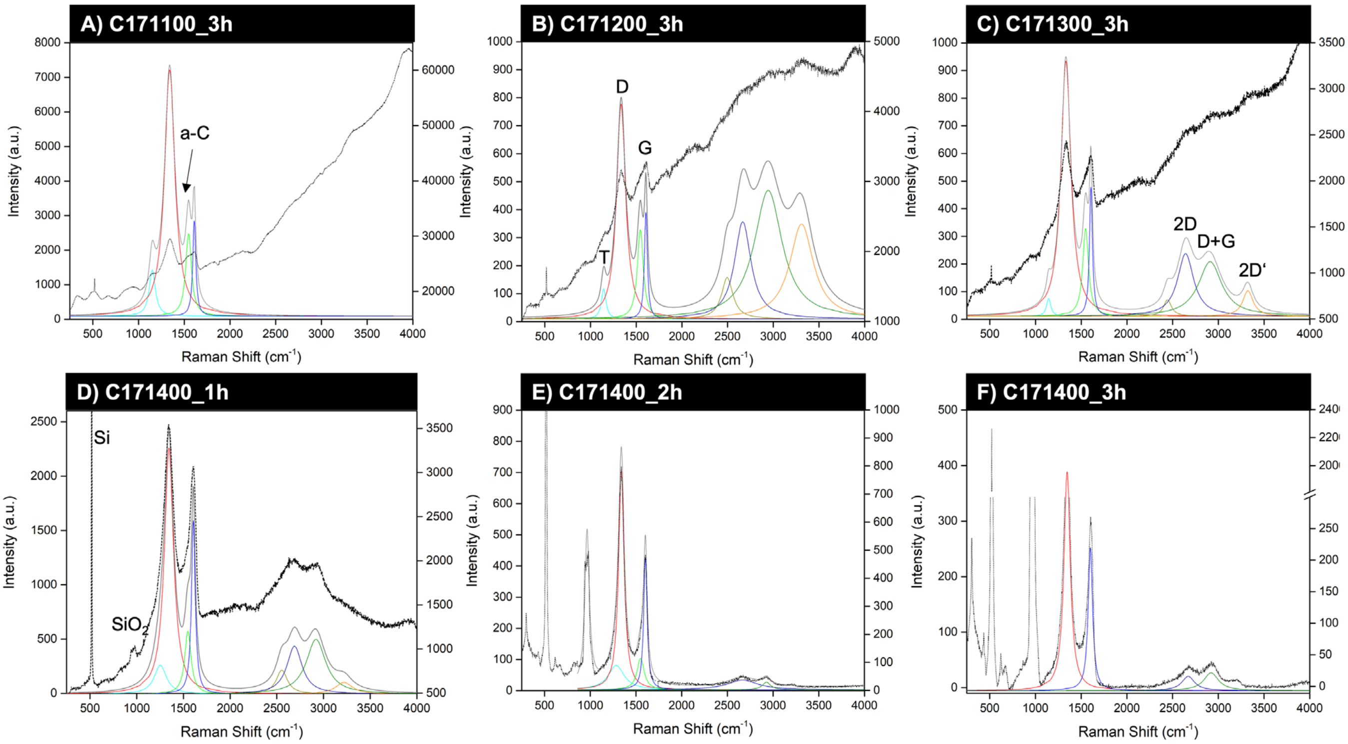

FIGURE 2 Lorentzian fitting of the Raman spectra of the matrix of the SiOC samples annealed at different temperatures and dwelling times. The untreated spectra are shown in black.

these bands has been made to extract indications about the quality and microstructure of carbon-based materials, including crystallinity and level of disorder revealed by the peak positions, peak shapes, and peak intensities.[30–33] Larouche et al. expanded the work by considering the tortuosity of carbon domains within the material and defining a new parameter, L_{eq} (see Equation (4)) by multiplying the tortuosity ratio with the lateral crystal size, L_a [34] (see Equation (1)). The works of Cançado et al. on quantifying defects have been the basis of the present study to calculate the defect density, n_D, and the distance between defects, L_D[30,31] (see Equations (2) and (3)).

$$L_a = \left(2.4 \times 10^{-10}\right) \lambda_L^4 \left(\frac{A_D}{A_G}\right)^{-1} \tag{1}$$

$$L_D^2 = 1.8\ x\ 10^{-9}\ \lambda_L^4 \frac{A_G}{A_D} \tag{2}$$

$$n_D = \frac{2.4\ x\ 10^{22} A_D}{\lambda_L^4 \qquad A_G} \tag{3}$$

$$L_{eq} = 77.0648 \frac{A_{2D}}{A_D.} \tag{4}$$

Looking at Figure 2, the untreated spectra in black exhibit high fluorescence background for the samples annealed at temperatures below 1400°C. The broad region concealing the second-order Raman region from 2400 cm^{-1} indicates the amorphous state of the samples. At 1400°C, increasing the dwelling time promotes better crystallinity in the samples while the peaks of Si and the silica coming from the substrate also become more pronounced. This can be related to the decreasing thickness of the film as the annealing temperature and dwelling time increase, which is indeed clear from the cross-sections of the samples shown in Figure 3. Using the area under the curve of each peak taken using the Lorentz fitting, the graphitization indices of the sp[2-h]ybridized carbon phase in the studied samples were assessed with the help of Equations (1)–(4) and are listed in Table 1. An improvement in the ratio between the D- and G- bands can be seen as the temperature and dwelling times increase. This is further supported by the increasing of the lateral crystallite size L_a, which improved by four times as the temperature increased from 1100°C to 1400°C. On the other hand, a decrease of the value of L_{eq} with increasing temperature is seen for the SiOC-based amorphous matrix of the film. Zooming into the values calculated from C17_1300_3h and C17_1400_1h samples, the L_a and the L_{eq} of both the matrix and the oxygen-depleted segregations are comparable in magnitudes. As the annealing temperature of the thin film increases, it is shown that the size of the carbon domains in the segregated areas increases faster than that of the sp2-hybridized carbon phase present in the amorphous matrix. This is in agreement with a previous study, in which was

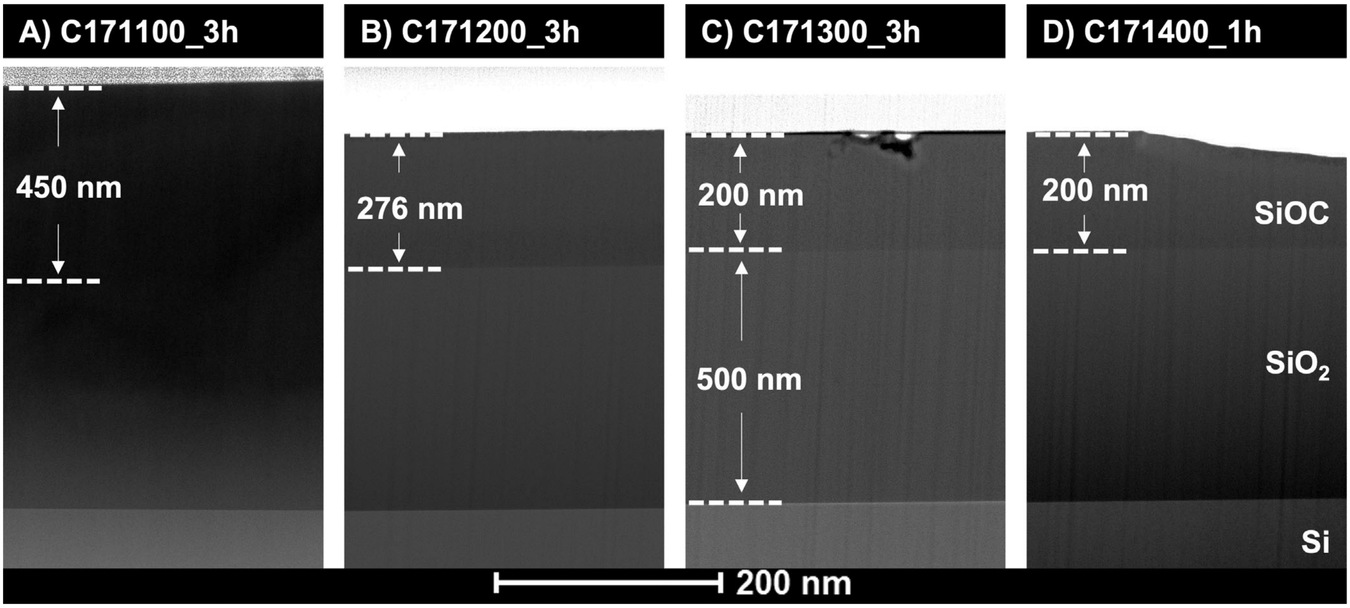

FIGURE 3 Cross-section of the matrices of SiOC film samples annealed at (A) 1100°C for 3 h, (B) 1200°C for 3 h, (C) 1300°C for 3 h, and (D) 1400°C for 1 h

TABLE 1 Graphitization indices of SiOC thin-film samples annealed at different temperatures and dwelling times. Indices were calculated using the Raman spectra using Equations (1), (2), (3) and (4)

Sample		A_D	A_G	A_{2D}	A_D/A_G	L_a (nm)	L_D (nm)	n_D ($\times$ 1012 cm^{-3})	L_{eq} (nm)
Matrix	C17_1100_3h	70.58	8.13	—	8.68	1.93	3.91	2.98	—
	C17_1200_3h	18.35	2.99	15.07	6.14	2.73	4.65	2.11	63.31
	C17_1300_3h	41.30	6.25	16.29	6.61	2.53	4.48	2.27	30.40
	C17_1400_1h	38.49	11.05	12.27	3.48	4.81	6.17	1.20	24.57
	C17_1400_2h	33.64	12.67	7.76	2.65	6.31	7.07	0.91	17.78
	C17_1400_3h	30.30	14.32	4.94	2.12	7.92	7.92	0.73	12.56
Precipitate	C17_1300_3h	41.30	6.25	16.29	6.61	2.53	4.48	2.27	30.40
	C17_1400_1h	30.76	8.51	8.45	3.62	4.63	6.06	1.24	21.17
	C17_1400_2h	36.99	11.34	18.41	3.26	5.13	6.38	1.12	38.35
	C17_1400_3h	18.30	15.21	18.22	1.20	13.93	10.50	4.14	76.74

also shown that the sp2-carbon in the segregations of the SiOC thin films is higher graphitized than the sp2-carbon from the amorphous matrix.[25]

The SiOC thin films on Si substrate were prepared for TEM and EELS analyses by preparing the cross-section via the FIB technique. Lamellae were taken along the matrices of the film, while additional lamellae were prepared for samples where oxygen-depleted segregations were evident. Displayed in Figure 3 are the cross-sections of samples annealed from 1100–1300°C for 3 h and the sample annealed at 1400°C for 1 h. The interfaces between the Si substrate, the SiO_2 passivation layer, and the SiOC film are clearly exposed after annealing at 1200°C. This method exposed the true thickness of the SiOC film at ≈200 nm. In the sample annealed at 1100°C, the amount of oxygen in the SiOC film gradually increases as it approaches the interface with the SiO_x passivation layer as shown in Figure S1. As the temperature increases, the thickness of the SiOC film decreases from 450 nm in the sample prepared at 1100°C to ≈200 nm in the sample annealed at 1400°C. At the same time, the oxygen-depleted segregations appear within the film. Interestingly, C17_1400_1h showed the development of a sinkhole, or a depression, leading to the segregations at the center, also shown in Figure 7A. The formation of the segregation started to manifest after annealing at 1300°C for 3 h.

EDS profiles of the cross-sections presented in Figure 3 are extracted to determine the diffusivity of carbon between the SiOC thin film and the SiO_x layers depicted in Figure 4. Using the Fick's second law of diffusion, the carbon diffusion constant (D_C) was estimated using Equation (5), where c_{max} and c_{min} are the initial concentrations

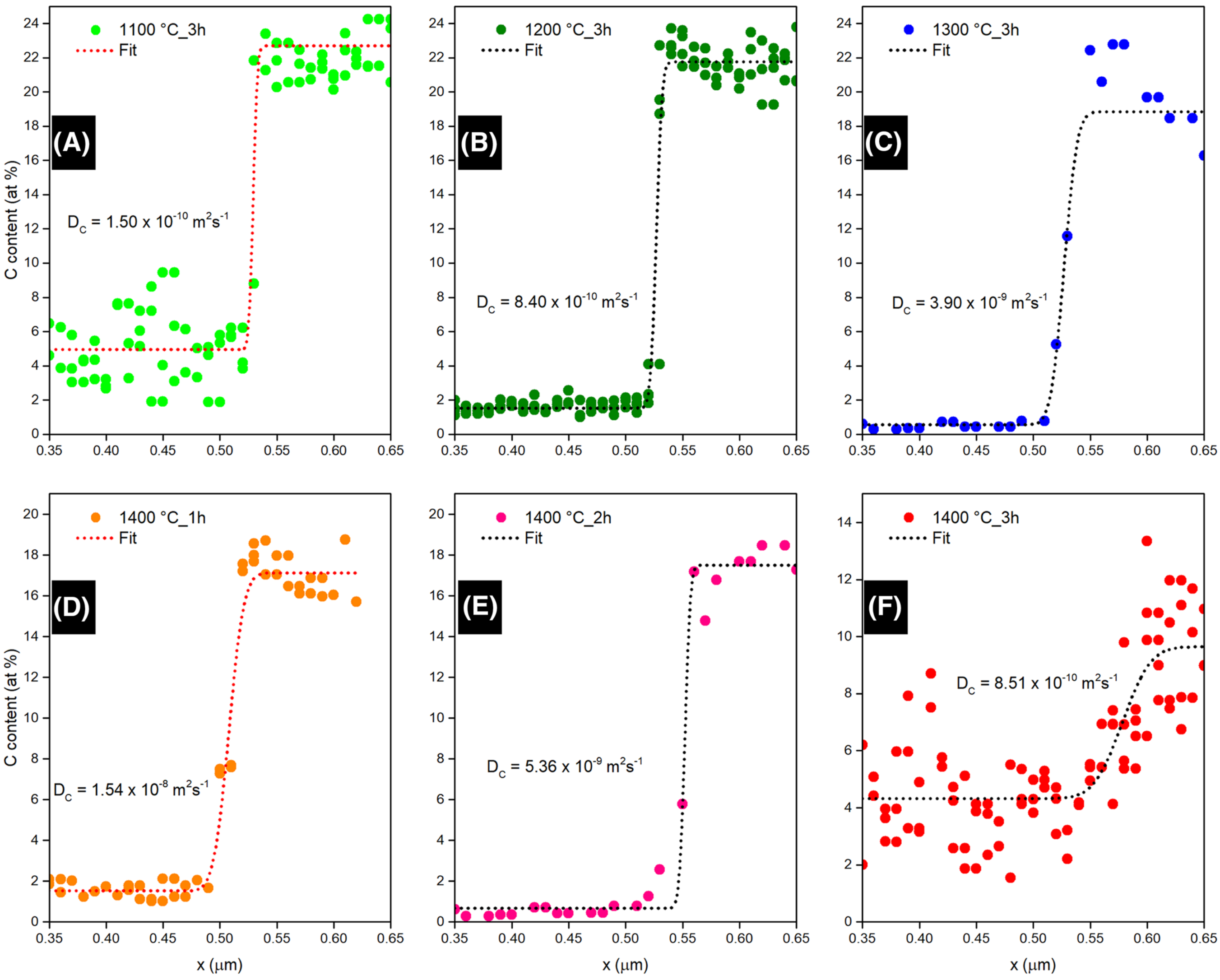

FIGURE 4 (A–C) Carbon profiles from EDS analysis and calculated coefficients of diffusion for SiOC thin film samples annealed at different temperatures, 1100–1300°C, at 3 h dwelling time. (D–F) Carbon profiles of isothermally annealed samples at 1400°C at different dwelling times, 1–3 h

at the interface between the SiOC film and the SiO_x passivation layer, x_0 corresponds to the inflection point of the profile, and t is annealing dwell time.

$$y\ (x,t) = \frac{c_{max}+c_{min}}{2} + \frac{c_{max}-c_{min}}{2}\mathrm{erf}\left(\frac{x-x_0}{2\sqrt{D_C t}}\right) \tag{5}$$

$$D_C = D_0 exp\left(-\frac{Q_d}{RT}\right) \tag{6}$$

Figure 4A–C displays the resulting carbon distribution after 3 h of annealing at temperatures 1100–1300°C, wherein the carbon concentration on the SiOC layer is sustained at ≈22 at%. In Figure 4D–F, isothermal annealing is performed at 1400°C at different dwelling times, 1–3 h. The resulting diffusion coefficients for the isothermally annealed samples exhibited an inverse proportionality with increasing dwelling time. The diffusion coefficient at 1400_3h sample is one magnitude lower than those for the other two samples annealed at 1400°C. This can be attributed to the low carbon concentration gradient between the film and SiO_x layer which is a result of the growth of C-rich segregations which are more prominent after 3 h of annealing at 1400°C. To keep the carbon concentration at an akin level, the 1400_1h sample is used to compare the diffusion coefficients of carbon at different temperatures.

Using the Arrhenius relation in Equation (6), wherein D_0 is the pre-exponential factor, Q_d is the activation energy, and R is the gas constant (8.31 J mol^{-1} K^{-1}), an exponential relationship of the diffusivity with temperature is observed in Figure 5A. The natural logarithm of the calculated D_C is

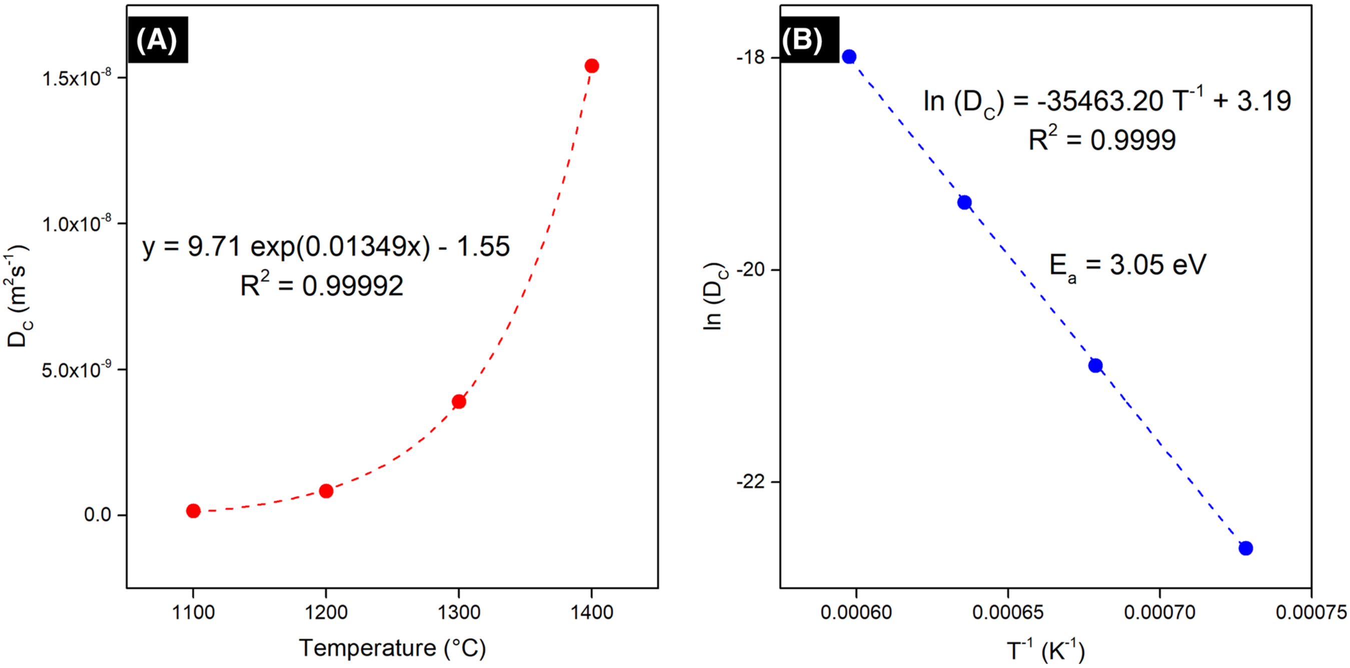

FIGURE 5 Diffusion coefficients of carbon obtained from EDS analysis of carbon profiles of SiOC thin film samples annealed at different isothermal temperatures (A) and the corresponding Arrhenius plot thereof (B)

then plotted against the inverse of temperature to extract the activation energy of the diffusing species which is shown in Figure 5B. The activation energy is extracted from the slope of the line of the Arrhenius plot resulting in 3.05 eV with an excellent fit of 99.99% and D_0 equal to 3.19. The calculated activation energy is comparable to the value of Shimoo et al.,[35] E_a^C = 3.74 eV, obtained from the reduction of SiO_2 with graphite leading to the formation of SiC and SiO as reduction products. In comparison, looking at the potential diffusivity of the three elements present in SiOC, the calculated E_a^C (3.05 eV) of carbon to silica is lower than the activation energy required to facilitate self-diffusion of Si to SiO_2 (E_a^{Si} = 4.56 eV)[35–37] but larger than the activation energy required to diffuse oxygen to silica (E_a^O = 2.54 eV).[38,39] Increasing the annealing temperature also promotes free carbon segregation which also increases the C/SiO_2 mixture ratio leading to a significant increase in the production of SiC. Consequently, with more time for annealing, the concentration of carbon left on the SiOC matrix diminishes slowing down the diffusivity of carbon which is evident in Figure 4D–F.

The EELS map and selected area electron diffraction (SAED) pattern of the graphitic carbon domains are presented in Figure 6. The Si $L_{2,3}$ edge, which is highly visible in all the spectra can be divided into the energy loss near edge structure (ELNES) at 120 eV with an onset at 104 eV, and the extended energy loss fine structure (EXELFS) at 150 eV which is superimposed with the L_1 edge.[40–43] The broadened peak at 120 eV is a result of the amorphous O-Si-C units within the region with the residual peak at 115 eV from the Si-O-Si bonds.[41,43] The absence of a sharp peak at 108 eV confirms the absence of SiO_2 within the C-rich area of the segregation.[40,42] Moreover, at the midpart of the map (black area), the C K-edge is predominantly composed of broad π^* peaks at 285 eV, which diminishes toward the gray area of the map with the rise of the σ^* peak ≈300 eV which suggests the existence of a mixture of sp2 and sp3 carbons.[19,41,44,45] The white region on the map exhibited peaks of N K-edge at 400 eV which supports the presence of Si_3N_4 within the segregation. In Figure 6B, the HRTEM image of the C-rich area along the (0003) basal plane exhibited the hexagonal rings of carbon structure with bent areas indicated by the white dashed lines. In conjunction with the Raman results in Table 1, these results support the tortuous nature of the carbon domains present in the film.

Two models to structurally describe the architecture of amorphous silicon oxycarbide have been proposed by Widgeon et al.[1] and Saha et al.,[46] respectively, focusing on the SiC_nO_{4-n}-based glassy network and the sp2-carbon phase. The work of Widgeon et al. described the structure of SiOC to follow a Swiss-cheese morphology composed of a fractal network and “voids.” The fractal network has the SiC_nO_{4-n} composition while the sp2-hybridized carbons are found within its voids. As deduced from Raman analysis, C17_1100_3h sample is in agreement with the model of Widgeon et al. with ~2 nm free carbon domains, although this is not easy to envision based on the SEM

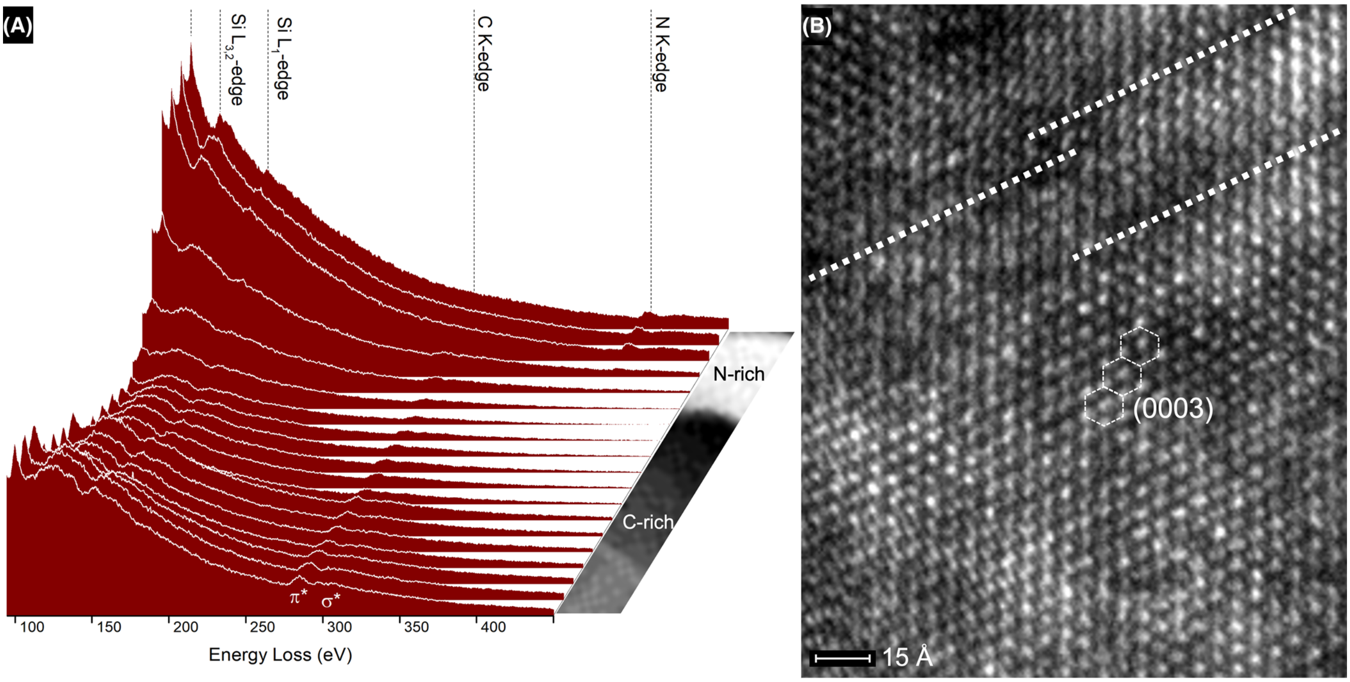

FIGURE 6 (A) EELS spectra of C17_1400_3h sample taken within the segregation region (C/SiC/N). (B) HAADF pattern of graphitic carbon taken along the (0003) plane. Dashed lines indicate the curved sections of the graphitic carbon formed within the segregation

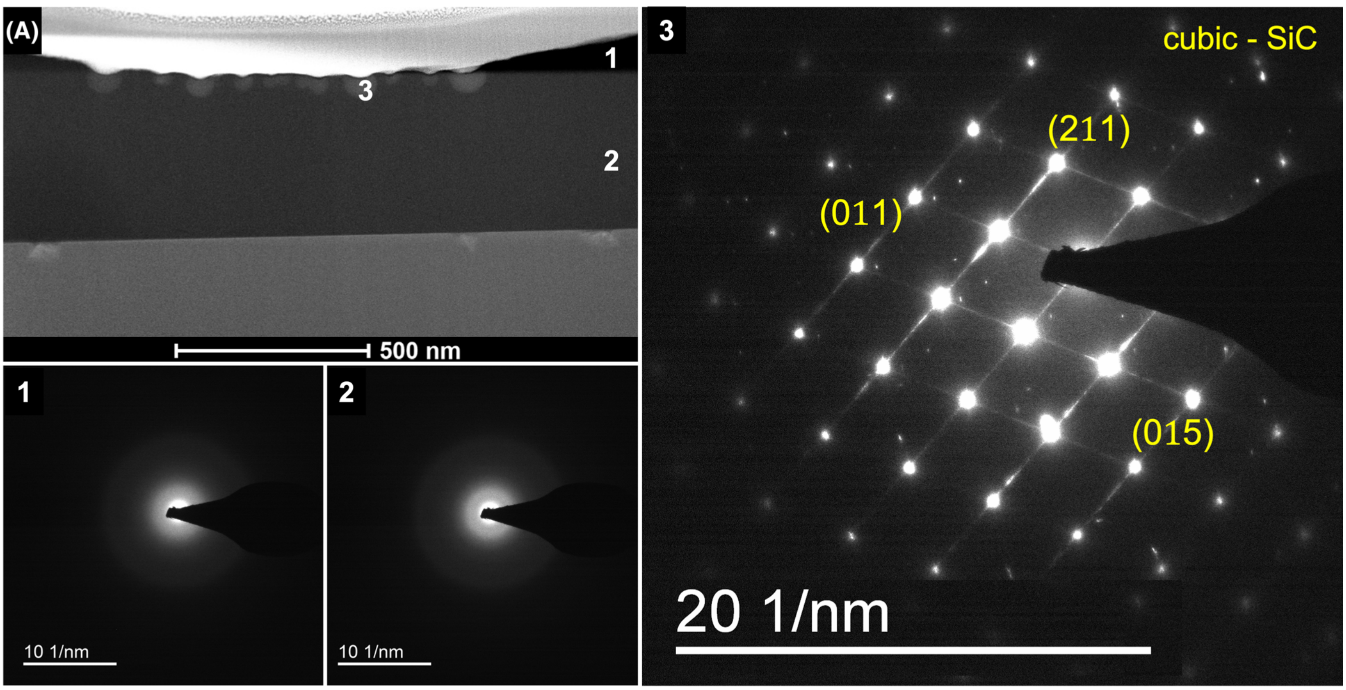

FIGURE 7 TEM image of C17_1400_1h sample with an evident thickness. SAED patterns of (1) SiOC film and (2) SiO2 layer remained in amorphous state while (3) stacking faults of SiC are found on the thickness-depleted area of the SiOC film.

image in Figure 1B. Relating to Figure 1B, the microstructure of the thin film synthesized in the present work at 1400°C agrees well with the model of Widgeon et al. on a microscale. It is considered that the formation of sp2-hybridized carbon serves as the main driving force for the generation of the carbon-rich segregations manifested on the thin film microstructure. The diffusivity suggests that increasing the annealing temperature promotes the

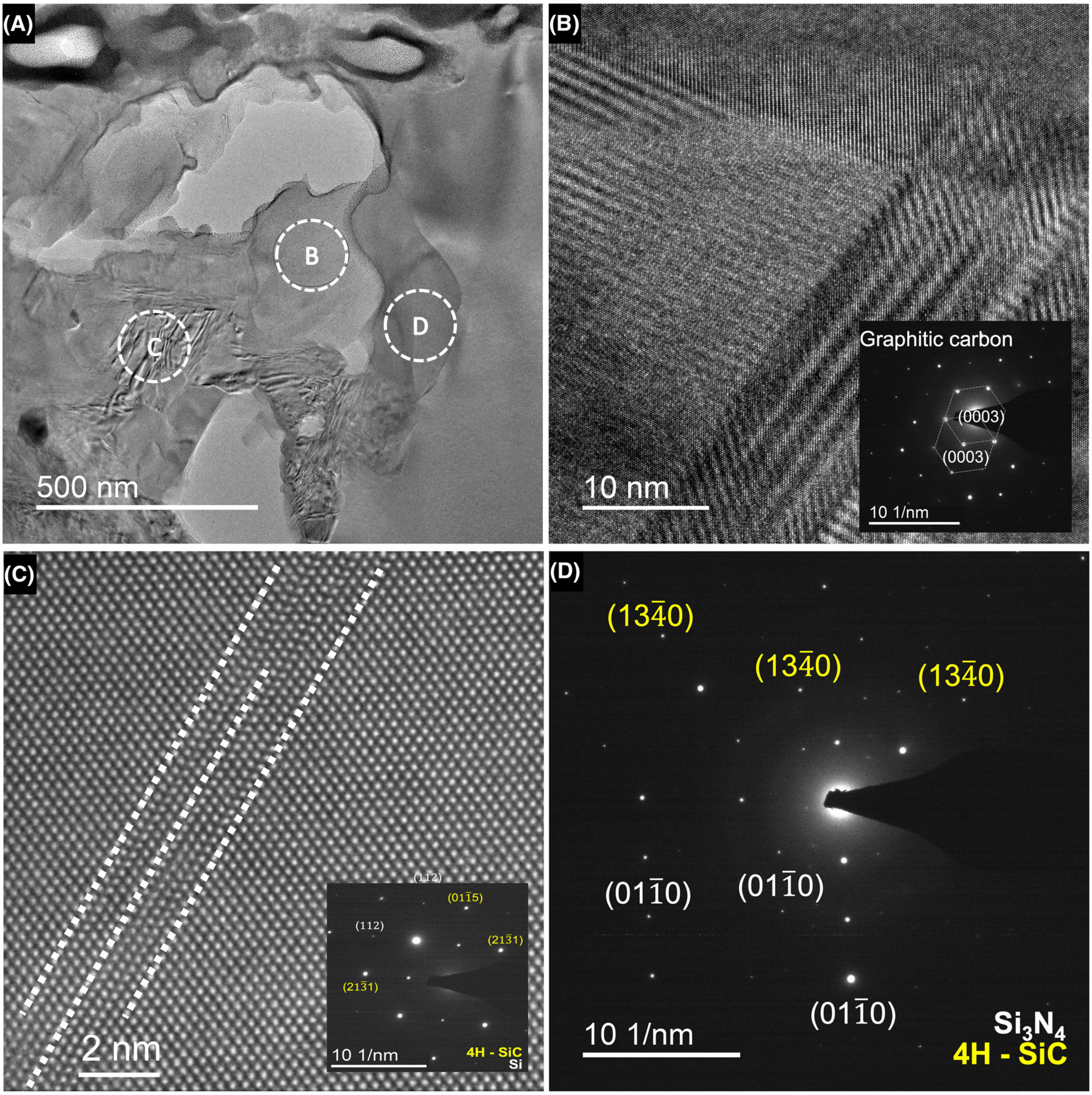

FIGURE 8 TEM image and SAED pattern of the carbon-rich area of the C17_1400_3h sample. (A) TEM image of C17_1400_3h sample segregation with equivalent SAED patterns. (B) Graphitic carbon; (C) 4H-SiC-rich region; (D) β-Si3N4-rich region

formation of SiC_nO_{4-n} structural units, which facilitates a migration path for the free carbons. With the benefit of the SiO_2 layer from the silicon substrate, after annealing at 1400°C for 1 h, diffusion of the carbon is highly favored leading to the formation of the microscale carbon-rich segregations denoted by the thickness depletion in Figure 7. The SAED pattern (3) confirms the presence of stacking faults of cubic-SiC on the interface of the SiOC film and the SiO_2 layer, while the rest of the SiOC film remains in an amorphous state (Figure 7_SAED Pattern 1). SAED Pattern 2 denotes the SiO_2 layer.

After 3 h of annealing at 1400°C, the segregation grows further down into the SiO_2 layer without reaching the Si substrate. In Figure 8, the segregation area is revealed to be composed of dense areas containing sp2-hybridized carbon domains, 4H-SiC, and β-Si_3N_4, which are presented with corresponding SAED patterns. The formation of Si_3N_4 is reasonable and is a consequence of the reaction of N_2 gas with the in situ formed $SiO_{4-x}C_x$. The reaction has a minimal contribution during the thermal decomposition of SiOC/Si/SiC and is more favored at temperature between 1400 and 1600°C.[47] It is obvious from the SAED patterns that multiple crystalline phases exist in the segregation. On the TEM image, it is apparent that 4H-SiC and β-Si_3N_4 exist as fragments distributed in the area of the segregation.

4 | CONCLUSIONS

In the present study involving several annealing temperatures and dwelling times, the SiOC thin-film displays two distinct phases of segregated round-shaped structures homogenously distributed in a matrix. These two phases are differentiated by the amount of carbon and oxygen contents making the segregation C-rich and O-depleted, whereas the matrix is O-rich. Through Raman analysis, non-destructive characterization of the carbon domains with the SiOC film is carried out revealing the domain of sp^2-hybridized carbons present on both the matrix and the segregations. Through this work, a clear manifestation of carbon domains is demonstrated, which correspondingly facilitates the formation of SiC via diffusion. Finally, increasing the annealing temperature demonstrated a positive trend in the growth mechanism of the microscale segregation composed of SiC, Si_3N_4, and graphitic carbon domains, which is confirmatory of the 2-level hierarchical microstructure of the SiOC film on a silicon substrate. The diffusion coefficient of carbon to silica showed a direct proportionality to increasing temperature and an Arrhenius relation resulting in activation energy of 3.05 eV.

AUTHOR CONTRIBUTIONS

Conceptualization: Emmanuel III Ricohermoso and Emanuel Ionescu; methodology, software, formal analysis, investigation, resources, and data curation: Emmanuel III Ricohermoso, Maxime Vallet, Eva Heripre, and Susana Solano-Arana; writing—original draft preparation: Emmanuel III Ricohermoso; writing—review and editing: Emanuel Ionescu and Ralf Riedel; visualization: Emmanuel III Ricohermoso; supervision: Emanuel Ionescu; project administration: Emmanuel III Ricohermoso, Maxime Vallet, and Emanuel Ionescu; funding acquisition: Emanuel Ionescu and Ralf Riedel. All authors have read and agreed to the published version of the manuscript.

ACKNOWLEDGMENTS

The authors gratefully acknowledge funding from the German Science Foundation (DFG Germany)—grant no. 411658150 (microstructured C/SiCX (X = O,N)-based high-temperature strain gauge). Additionally, Emanuel Ionescu acknowledges funding from DFG within the Heisenberg program (IO 64/1). The authors would also like to thank Dr. Maxime Vallet for his assistance for the TEM measurements.

Open access funding enabled and organized by Projekt DEAL.

CONFLICT OF INTEREST

The authors declare no conflict of interest.

ORCID

Emmanuel III Ricohermoso https://orcid.org/0000-0002-4093-4751
Ralf Riedel https://orcid.org/0000-0001-6888-7208
Emanuel Ionescu https://orcid.org/0000-0002-3266-3031

REFERENCES

1. Widgeon SJ, Sen S, Mera G, Ionescu E, Riedel R, Navrotsky A. 29Si and 13C solid-state NMR spectroscopic study of nanometer-scale structure and mass fractal characteristics of amorphous polymer derived silicon oxycarbide ceramics. Chem Mater. 2010;22(23):6221–8.
2. Ionescu E, Mera G, Riedel R. Polymer-derived ceramics: materials design towards applications at ultrahigh-temperatures and in extreme environments. In: Nanotechnology: Concepts, methodologies, tools, and applications. IGI Global; 2014. p. 1108–39.
3. Mera G, Navrotsky A, Sen S, Kleebe HJ, Riedel R. Polymer-derived SiCN and SiOC ceramics – structure and energetics at the nanoscale. J Mater Chem A. 2013;1(12):3826–36.
4. Mera G, Gallei M, Bernard S, Ionescu E. Ceramic nanocomposites from tailor-made preceramic polymers. Nanomaterials (Basel). 2015;5(2):468–540.
5. Babonneau F, Soraru GD, D'Andrea G, Dire S, Bois L. Silicon oxycarbide glasses from sol-gel precursors. MRS Online Proceedings Library (OPL). 1992;271:789.
6. Kalfat R, Babonneau F, Gharbi N, Zarrouk H. 29 Si MAS NMR investigation of the pyrolysis process of cross-linked polysiloxanes prepared from polymethylhydrosiloxane. J Mater Chem. 1996;6(10):1673–8.
7. Trimmel G, Badheka R, Babonneau F, Latournerie J, Dempsey P. Solid state NMR and TG/MS study on the transformation of methyl groups during pyrolysis of preceramic precursors to SiOC glasses - ProQuest. J Sol-Gel Sci Technol. 2003;26(1–3):279–83.
8. Rosenburg F, Balke B, Nicoloso N, Riedel R, Ionescu E. Effect of the content and ordering of the sp2 free carbon phase on the charge carrier transport in polymer-derived silicon oxycarbides. Molecules. 2020;25(24):5919.
9. Weinmann M, Ionescu E, Riedel R, Aldinger F. Chapter 11.1.10 - Precursor-Derived Ceramics*. In: Somiya S, editor. Handbook of advanced ceramics. 2nd ed. Oxford: Academic Press; 2013. p. 1025–101.
10. Ionescu E, Kleebe HJ, Riedel R. Silicon-containing polymer-derived ceramic nanocomposites (PDC-NCs): preparative approaches and properties. Chem Soc Rev. 2012;41(15):5032–52.

11. Felix Rosenburg, Emanuel Ionescu, Norbert Nicoloso, Ralf Riedel. High-temperature Raman spectroscopy of nano-crystalline carbon in silicon oxycarbide. Materials. 2018;11(1):93.
12. Roth F, Waleska P, Hess C, Ionescu E, Nicoloso N. UV Raman spectroscopy of segregated carbon in silicon oxycarbides. J Ceram Soc Japan. 2016;124(10):1042–5.
13. Colombo P, Mera G, Riedel R, Sorarù GD. Polymer-derived ceramics: 40 years of research and innovation in advanced ceramics. J Am Ceram Soc. 2010;93(7):1805–37.
14. Riedel R, Mera G, Hauser R, Klonczynski A. Silicon-based polymer-derived ceramics: synthesis properties and applications-a review: dedicated to Prof. Dr. Fritz Aldinger on the occasion of his 65th birthday. Nippon Seramikkusu Kyokai Gakujutsu Ronbunshi. 2006;114(1330):425–44.
15. Kleebe HJ, Turquat C, Sorarù GD. Phase separation in an SiCO glass studied by transmission electron microscopy and electron energy-loss spectroscopy. J Am Ceram Soc. 2001;84(5):1073–80.
16. Chomel AD, Dempsey P, Latournerie J, Hourlier-Bahloul D, Jayasooriya UA. Gel to glass transformation of methyltriethoxysilane: a silicon oxycarbide glass precursor investigated using vibrational spectroscopy. Chem Mater. 2005;17(17):4468–73.
17. Sorarù GD, D'Andrea G, Glisenti A. XPS characterization of gel-derived silicon oxycarbide glasses. Mater Lett. 1996;27(1):1–5.
18. Sorarù GD. Silicon oxycarbide glasses from gels: Code: H1. J Sol-Gel Sci Technol. 1994;2(1–3):843–8.
19. Giuliano G, Hans-Joachim K, D BY, Florence B. Evolution of C-rich SiOC ceramics Part II. Characterization by high lateral resolution techniques: electron energy-loss spectroscopy, high-resolution TEM and energy-filtered TEM. Int J Mater Res. 2006;97(6):710–20.
20. Sorarù GD, Modena S, Guadagnino E, Colombo P, Egan J, Pantano C. Chemical durability of silicon oxycarbide glasses. J Am Ceram Soc. 2002;85(6):1529–36.
21. Bois L, Maquet J, Babonneau F, Bahloul D. Structural characterization of sol-gel derived oxycarbide glasses. 2. Study of the thermal stability of the silicon oxycarbide phase. Chem Mater. 1995;7(5):975–81.
22. Bréquel H, Parmentier J, Walter S, Badheka R, Trimmel G, Masse S, et al. Systematic structural characterization of the high-temperature behavior of nearly stoichiometric silicon oxycarbide glasses. Chem Mater. 2004;16(13):2585–98.
23. Saha A, Raj R. Crystallization maps for SiCO amorphous ceramics. J American Ceramic Society. 2007;90(2):578–83.
24. Ricohermoso E, Klug F, Schlaak H, Riedel R, Ionescu E. Electrically conductive silicon oxycarbide thin films prepared from preceramic polymers. Int J Appl Ceram Technol. 2021;19(1):149–64.
25. Ricohermoso E, Klug F, Schlaak H, Riedel R, Ionescu E. Compressive thermal stress and microstructure-driven charge carrier transport in silicon oxycarbide thin films. J Eur Ceram Soc. 2021;41(13):6377–84.
26. Reich S, Thomsen C. Raman spectroscopy of graphite. Phil Trans R Soc A: Math, Phys Eng Sci. 2004;362(1824):2271–88.
27. Kostić R, Mirić M, Radić T, Radović M, Gajić R, Popović ZV. Optical characterization of graphene and highly oriented pyrolytic graphite. Acta Phys Pol A. 2009;116(4):718–21.
28. Rousseau DL, Bauman RP, Porto SPS. Normal mode determination in crystals. J Raman Spectrosc. 1981;10(1):253–90.
29. Saito R, Jorio A, Souza Filho AG, Dresselhaus G, Dresselhaus MS, Pimenta MA. Probing phonon dispersion relations of graphite by double resonance Raman scattering. Phys Rev Lett. 2002;88(2):027401.
30. Cançado LG, Takai K, Enoki T, Endo M, Kim YA, Mizusaki H, et al. General equation for the determination of the crystallite size La of nanographite by Raman spectroscopy. Appl Phys Lett. 2006;88(16):163106.
31. Cançado LG, Jorio A, Ferreira EHM, Stavale F, Achete CA, Capaz RB, et al. Quantifying defects in graphene via Raman spectroscopy at different excitation energies. Nano Lett. 2011;11(8):3190–6.
32. Bokobza L, Bruneel JL, Couzi M. Raman spectra of carbon-based materials (from graphite to carbon black) and of some silicone composites. C. 2015;1(1):77–94.
33. Baranov AV, Bekhterev AN, Bobovich YaS, Petrov VI. Interpretation of certain characteristics in Raman spectra of graphite and glassy carbon. Opt Spectrosc. 1987;62:612–6.
34. Larouche N, Stansfield BL. Classifying nanostructured carbons using graphitic indices derived from Raman spectra. Carbon. 2010;48(3):620–9.
35. Shimoo T, Mizutaki F, Ando S, Kimura H. Kinetics of reduction of silica with graphite. J Jpn Inst Met. 1988;52(10):945–53.
36. Estreicher SK, Backlund DJ, Carbogno C, Scheffler M. Activation energies for diffusion of defects in silicon: the role of the exchange-correlation functional. Angew Chem Int Ed. 2011;50(43):10221–5.
37. Bracht H. Self- and foreign-atom diffusion in semiconductor isotope heterostructures. I. Continuum theoretical calculations. Phys Rev B. 2007;75(3):035210.
38. di Ventra M, Pantelides ST. Oxygen stability, diffusion, and precipitation in SiC: implications for thin-film oxidation. Journal of Elec Materi. 2000;29(3):353–8.
39. Gösele U, Tan TY. Oxygen diffusion and thermal donor formation in silicon. Appl Phys A. 1982;28(2):79–92.
40. Wang YY, Chan SF, Jin Q, Zhuang K, Choi JK. A method of using Si L-edge for O/Si and N/Si quantitative ratio analysis by electron energy loss spectroscopy (EELS). Micron. 2021;146:103065.
41. Schneider R, Woltersdorf J, Lichtenberger O. Phase identification in composite materials by EELS fine-structure analysis. J Microsc. 1996;183(1):39–44.
42. Garvie L, Buseck P. Bonding in silicates: Investigation of the Si L2,3 edge by parallel electron energy-loss spectroscopy. Am Mineral. 1999;84:946–64.
43. Pippel E, Lichtenberger O, Woltersdorf J. Identification of silicon oxycarbide bonding in Si-C-O-glasses by EELS. J Mater Sci Lett. 2000;19:2059–60.
44. Edalati K, Daio T, Ikoma Y, Arita M, Horita Z. Graphite to diamond-like carbon phase transformation by high-pressure torsion. Appl Phys Lett. 2013;103(3):034108.
45. Ponsonnet L, Donnet C, Varlot K, Martin JM, Grill A, Patel V. EELS analysis of hydrogenated diamond-like carbon films. Thin Solid Films. 1998;319(1):97–100.
46. Saha A, Raj R, Williamson DL. A model for the nanodomains in polymer-derived SiCO. J Am Ceram Soc. 2006;89(7):2188–95.

47. Osip H, Czosnek C, Janik JF, Marchewka J, Sitarz M. Amorphous silicon oxynitride-based powders produced by spray pyrolysis from liquid organosilicon compounds. Materials (Basel). 2021;14(2):386.

SUPPORTING INFORMATION

Additional supporting information can be found online in the Supporting Information section at the end of this article.

How to cite this article: Ricohermoso E, Heripre E, Solano-Arana S, Riedel R, Ionescu E. Hierarchical microstructure growth in a precursor-derived SiOC thin film prepared on silicon substrate. Int J Appl Ceram Technol. 2023;20:735–746. https://doi.org/10.1111/ijac.14185